submitted to *Geophys. J. Int.*

Separating GIA signal from surface mass change using GPS and GRACE data

Bramha Dutt Vishwakarma[1,2], Yann Ziegler[2], Jonathan L. Bamber[2,3], Sam Royston[2]

[1] *Interdisciplinary Centre for Water Research, Indian Institute of Science, Bangalore, India*

[2] *School of Geographical sciences, University of Bristol, UK* [3] *AI4EO Future Lab, Technical University of Munich, Germany*

Received ; in original form

SUMMARY

The visco-elastic response of the solid Earth to the past glacial cycles and the present day surface mass change (PDSMC) are detected by the geodetic observation systems such as global navigation satellite system (GNSS) and satellite gravimetry. Majority of the contemporary PDSMC is driven by climate change and in order to better understand them using the aforementioned geodetic observations, glacial isostatic adjustment (GIA) signal should be accounted first. The default approach is to use forward GIA models that use uncertain ice-load history and approximate Earth rheology to predict GIA, yielding large uncertainties. The proliferation of contemporary, global, geodetic observations and their coverage have therefore enabled estimation of data-driven GIA solutions. A novel framework is presented that uses geophysical relations between the vertical land motion (VLM) and geopotential anomaly due to GIA and PDSMC to express GPS VLM trends and GRACE geopotential trends as a function of either GIA or PDSMC, which can be easily solved using least-squares regression. The GIA estimates are data-driven and differ significantly from forward models over Alaska and Greenland.

Key words: Geopotential theory, Global change from geodesy, Loading of the Earth, Satellite geodesy.

1 INTRODUCTION

Glacial isostatic adjustment (GIA) is the visco-elastic response of the solid Earth to past glacial changes (Farrell and Clark, 1976; Peltier, 2004). This process is partly responsible for the observed secular vertical land motion (VLM) over parts of North America, Scandinavia, Greenland and Antarctica (Peltier et al., 2015; Ivins et al., 2013; Horwath et al., 2012; Simon et al., 2017). GIA also affects the gravity field of the Earth and therefore is observed by the Gravity Recovery And Climate Experiment (GRACE) satellite mission (Wahr et al., 1998; Tapley et al., 2019). GRACE data is known for highlighting the contemporary surface mass redistribution, which can only be estimated after correcting for GIA (Peltier, 2009). Therefore, the accuracy of GIA estimate is critical for assessing PDSMC accurately, for example, GIA alone is suspected to explain 50 % of the total mass change over Antarctica (Caron and Ivins, 2020). Similarly, the accuracy of GIA is also critical for assessing Greenland ice-sheet mass balance, sea level rise, and land hydrology related mass redistribution processes (Martín-Español et al., 2016; Shepherd et al., 2018; WCRP, 2018; Willen et al., 2020). Since GIA is a response of the solid Earth to the past loading and unloading, forward models have been developed that predict GIA signal with the help of an approximate ice-load history and Earth rheology (Peltier, 2004; Geruo et al., 2013; Ivins et al., 2013). The uncertainties in these GIA forward models are sensitive to changes in input parameters and therefore several recent research studies advocated obtaining data-driven GIA estimates that are largely independent of approximations and assumptions on ice-load history (Wu et al., 2010; Wang et al., 2013; Hill et al., 2010; Martín-Español et al., 2016; Simon et al., 2017; Sasgen et al., 2017; Whitehouse, 2018; Gao et al., 2019).

The possibility for obtaining a data-driven GIA estimate was first realised when GRACE mission was in preparation. In a simulation, Wahr et al. (2000) demonstrated that GIA and the present day surface mass change (PDSMC) can be co-estimated from Ice, Cloud, and land Elevation Satellite (ICESat) and GRACE data. GRACE mission observes changes in the gravitational potential, which can be converted to surface mass change, while ICESat measured changes in the surface elevation that explain ice processes and bedrock movement (or VLM). It is to be noted that the surface mass change (ice, water) and non-surface processes (such as GIA) are related to perturbations in gravitational potential and VLM differently (Chao, 2016). It was in 2009 that the method by Wahr et al. (2000) was first implemented on real data over Antarctica (Riva et al., 2009). Since then, several contributions have improved on Riva et al. (2009) or Wahr et al. (2000) by either incorporating additional processes and better data or by employing new inversion techniques that may rely on constraints from GIA forward models (Velicogna and Wahr, 2002; Wu et al., 2010; Wang et al., 2013; Gunter et al., 2014; Rietbroek et al., 2016; Zou and Jin, 2016; Martín-Español et al., 2016; Sasgen et al., 2017; Simon et al., 2017; Gao et al., 2019; Sun and Riva, 2020). Recently, global navigation satellite system (GNSS) based VLM changes have been also integrated with either GRACE data or hydrological models to determine Centre of figure of the Earth, validate GIA models, and estimate PDSMC or GIA signal (Blewitt, 2003; Davis et al., 2004; Tregoning et al., 2009; Razeghi et al., 2019; Schumacher et al., 2018; Whitehouse, 2018; Argus et al., 2020).

In this article, we employ the approximate relations between VLM and respective surface and sub-surface processes to express the GPS observed VLM trends as a linear combination of PDSMC and GIA trends. After rearranging these relations, we are able to express observations in terms of spherical harmonic coefficients representing either PDSMC or GIA, which can be solved using least-squares regression. In a synthetic closed-loop experiment we demonstrate that our method works very well when the GNSS network is global and homogeneous in space, which is not true in reality. Large spatial gaps in GNSS data availability results in noisy estimates. Therefore, we propose to plug the gaps by augmenting GNSS data by estimating GNSS-equivalent VLM from a forward GIA model and GRACE data, which helps us obtain a stable solution for GIA and PDSMC. This approach is equivalent to using a forward model as an informative prior and updating it with observations. We also demonstrate that the choice of prior GIA model has a negligible effect on the output where we have GPS data. Since, there is a decent availability of GPS stations in and near GIA dominated regions, our GIA estimate is heavily data-driven. Nevertheless, we acknowledge that we rely on certain assumptions and approximation, such as we assume negligible VLM due to processes other than GIA and PDSMC, which may result in a few caveats that have also been explained. We show that our estimates are coherent with expected GIA signal for North America and Fennoscandia. Our GIA estimates differ significantly from two popular GIA models over Alaska and slightly over Greenland and Antarctica. This study demonstrates a novel mathematical framework to separate GIA and PDSMC trends in contemporary Earth observation dataset without relying heavily on prior GIA model or ice-load history.

2 MATHEMATICAL FRAMEWORK

Figure 1 illustrates the vertical (radial) component of the elastic and visco-elastic response of the solid Earth with respect to the centre of Mass of the Earth system. Let us suppose that a point $P(\theta, \lambda)$ on the surface of the Earth moves in the vertical direction by u in time t and this is recorded by a GNSS station. θ is the co-latitude and λ is the longitude. This vertical land movement (VLM) in the frame of centre of figure of the Earth can be written as a sum of elastic deformation (u_e) due to PDSMC and a viscous solid-Earth response (u_v) driven by GIA, assuming that other processes are either accounted for or are negligible ($\delta \approx 0$):

$$\Delta u(\theta, \lambda, t) = \Delta u_e(\theta, \lambda, t) + \Delta u_v(\theta, \lambda, t) + \delta(\theta, \lambda, t). \tag{1}$$

The linear rate of elastic VLM, $\dot{u}_e$ can be obtained from dimensionless Stokes coefficients for PDSMC ($\Delta\dot{C}^p_{\ell m}$ and $\Delta\dot{S}^p_{\ell m}$) as (Farrell, 1972; Davis et al., 2004; van Dam et al., 2007; Vishwakarma et al., 2020b)

$$\Delta\dot{u}_e(\theta, \lambda) = R \sum_{\ell,m} \frac{h'_\ell}{1+k'_\ell} \tilde{P}_{\ell m}(\cos\theta) \left[\Delta\dot{C}^p_{\ell m}\cos(m\lambda) + \Delta\dot{S}^p_{\ell m}\sin(m\lambda)\right], \tag{2}$$

where h'_ℓ and k'_ℓ are the elastic load Love numbers of degree ℓ, $\tilde{P}_{\ell m}$ are normalized Legendre functions of degree ℓ and order m. Theoretically ℓ goes from 0 to ∞ and m goes from 0 to ℓ, however, due to limited spatial sampling we truncate at a maximum degree L. R is the mean radius of the Earth in the same units as u_e. The viscous response due to GIA is known to be generated by flow of mantle material and the rate of VLM due to GIA ($\dot{u}_v$), like any surface deformation field, can be expanded in terms of dimensionless Stokes coefficients using spherical harmonic (SH) analysis (Purcell et al., 2011):

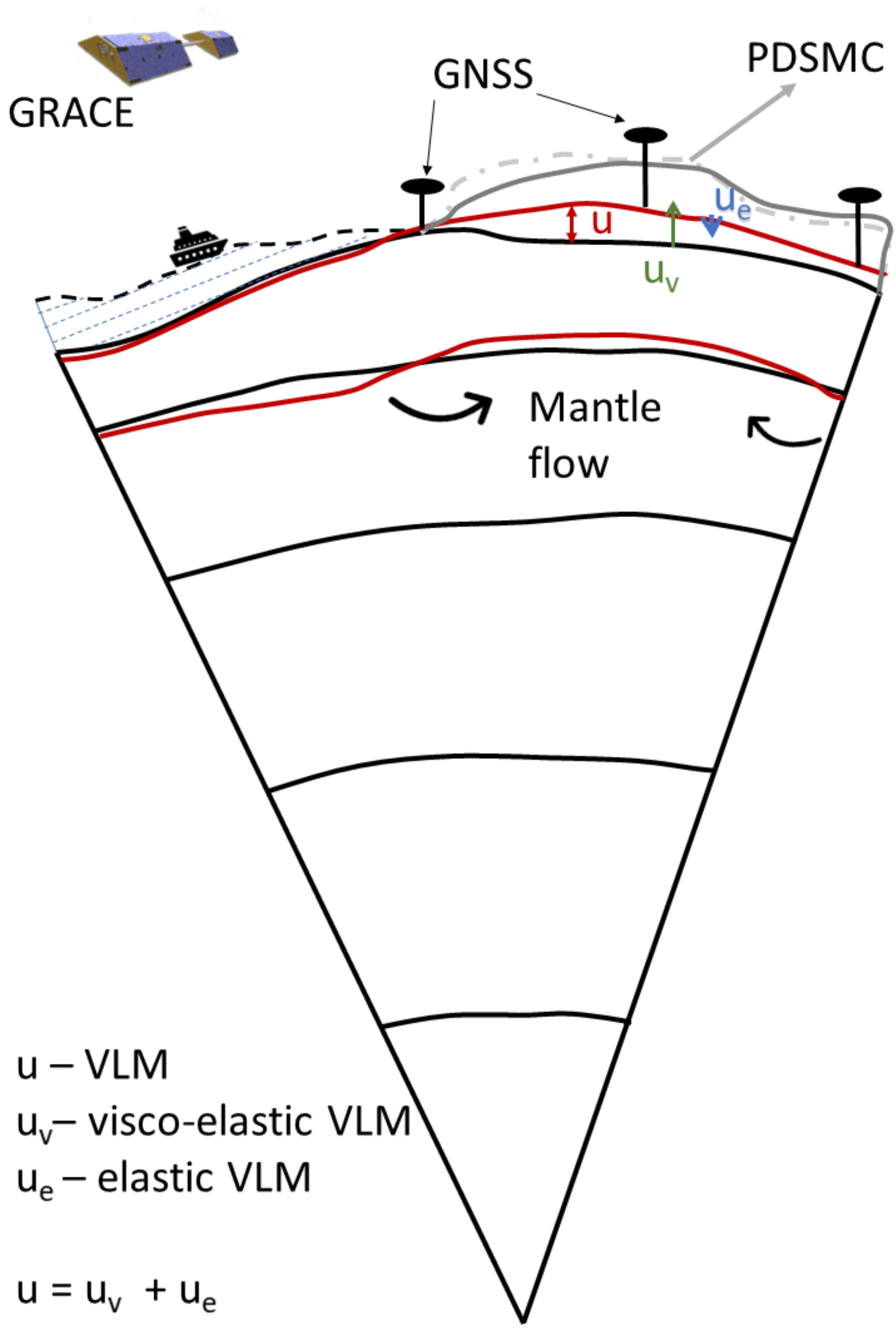

Figure 1. Illustration of solid Earth processes that result in vertical land deformation. The black line represents initial state of the bedrock and the red line represents the state after time t. Dotted grey to solid gray represents any surface mass change over continents in the same time period.

$$\Delta\dot{u}_v(\theta,\lambda) = R\sum_{\ell,m}(1.1677\ell - 0.5233)\tilde{P}_{\ell m}(\cos\theta)\left[\Delta\dot{C}^G_{\ell m}\cos(m\lambda) + \Delta\dot{S}^G_{\ell m}\sin(m\lambda)\right], \quad (3)$$

where $\Delta\dot{C}^G_{\ell m}$ and $\Delta\dot{S}^G_{\ell m}$ represent the rate of change in Stokes coefficients representing GIA related potential perturbation. Since for GRACE products we assume that all the mass redistribution takes place near the Earth's surface, i.e. $\approx$ within 10 km, and any changes in the mantle are beyond the thin layer assumption (Chao, 2016), a small error is inevitable that we assume to be negligible in this study. Adding (2) and (3),

$$\begin{aligned}\Delta\dot{u}(\theta,\lambda) = R\sum_{\ell,m}\Bigg\{&\frac{h'_\ell}{1+k'_\ell}\tilde{P}_{\ell m}(\cos\theta)\left[\Delta\dot{C}^p_{\ell m}\cos(m\lambda) + \Delta\dot{S}^p_{\ell m}\sin(m\lambda)\right]\\ &+ (1.1677\ell - 0.5233)\tilde{P}_{\ell m}(\cos\theta)\left[\Delta\dot{C}^G_{\ell m}\cos(m\lambda) + \Delta\dot{S}^G_{\ell m}\sin(m\lambda)\right]\Bigg\}. \quad (4)\end{aligned}$$

Let's write $\dot{u}(\theta,\lambda)$ as $\dot{u}(\cdot)$ from now on. Adding $\sum_{\ell,m}\frac{h'_\ell}{1+k'_\ell}\tilde{P}_{\ell m}(\cos\theta)\left[\Delta\dot{C}^G_{\ell m}\cos(m\lambda)+\Delta\dot{S}^G_{\ell m}\sin(m\lambda)\right]$ to the first half of (4) and subtracting the same from the second half and then rearranging it, we get

$$\begin{aligned}\Delta\dot{u}(\cdot) = R\sum_{\ell,m}\Bigg\{&\frac{h'_\ell}{1+k'_\ell}\tilde{P}_{\ell m}(\cos\theta)\left[\left(\Delta\dot{C}^p_{\ell m} + \Delta\dot{C}^G_{\ell m}\right)\cos(m\lambda) + \left(\Delta\dot{S}^p_{\ell m} + \Delta\dot{S}^G_{\ell m}\right)\sin(m\lambda)\right]\\ &+ \left(1.1677\ell - 0.5233 - \frac{h'_\ell}{1+k'_\ell}\right)\tilde{P}_{\ell m}(\cos\theta)\left[\Delta\dot{C}^G_{\ell m}\cos(m\lambda) + \Delta\dot{S}^G_{\ell m}\sin(m\lambda)\right]\Bigg\}. \quad (5)\end{aligned}$$

Combining Stokes coefficients for PDSMC and GIA gives

$$\left\{\begin{array}{c}\Delta\dot{C}_{\ell m}\\ \Delta\dot{S}_{\ell m}\end{array}\right\} = \left\{\begin{array}{c}\Delta\dot{C}^p_{\ell m} + \Delta\dot{C}^G_{\ell m}\\ \Delta\dot{S}^p_{\ell m} + \Delta\dot{S}^G_{\ell m}\end{array}\right\}, \quad (6)$$

where $\Delta\dot{C}_{\ell m}$ and $\Delta\dot{S}_{\ell m}$ are readily available from GRACE products. Using (6) in the first half of (5) gives us

$$\Delta\dot{u}(\cdot) = R\sum_{\ell,m}\left\{\frac{h'_\ell}{1+k'_\ell}\tilde{P}_{\ell m}(\cos\theta)\left[\Delta\dot{C}_{\ell m}\cos(m\lambda)+\Delta\dot{S}_{\ell m}\sin(m\lambda)\right]\right.$$
$$\left. + \left(1.1677\ell - 0.5233 - \frac{h'_\ell}{1+k'_\ell}\right)\tilde{P}_{\ell m}(\cos\theta)\left[\Delta\dot{C}^{G}_{\ell m}\cos(m\lambda)+\Delta\dot{S}^{G}_{\ell m}\sin(m\lambda)\right]\right\}. \quad (7)$$

The left hand side of (7) can be obtained from GNSS network, the first term on the right hand side can be obtained from GRACE and thus we can solve for the GIA SH coefficients.

Similarly and conversely, to solve for PDSMC, adding $\sum_{\ell,m}(1.1677\ell-0.5233)\tilde{P}_{\ell m}(\cos\theta)\Big[\Delta\dot{C}^{p}_{\ell m}\cos(m\lambda)+\Delta\dot{S}^{p}_{\ell m}\sin(m\lambda)\Big]$ to the first term of (4) and subtracting the same from the second term and then rearranging it, we can obtain

$$\Delta\dot{u}(\cdot) = R\sum_{\ell,m}\left\{(1.1677\ell - 0.5233)\tilde{P}_{\ell m}(\cos\theta)\left[\Delta\dot{C}_{\ell m}\cos(m\lambda)+\Delta\dot{S}_{\ell m}\sin(m\lambda)\right]\right.$$
$$\left. + \left[\frac{h'_\ell}{1+k'_\ell} - (1.1677\ell - 0.5233)\right]\tilde{P}_{\ell m}(\cos\theta)\left[\Delta\dot{C}^{p}_{\ell m}\cos(m\lambda)+\Delta\dot{S}^{p}_{\ell m}\sin(m\lambda)\right]\right\}. \quad (8)$$

2.1 Closed loop test

We test the framework in a closed loop environment with the help of synthetic dataset that is generated to mimic the geophysical processes we are interested in. We use the VLM predictions from Caron et al. (2018) GIA model to represent u_v, and u_e is obtained by using (2) on PDSMC estimates from GRACE data that has been corrected for GIA using the ICE-6G GIA model (Peltier et al., 2015). The GRACE level 2 data from the Institute of Geodesy, University of Graz, has been used in this study (Mayer-Gürr et al., 2018). The total VLM u is a sum of u_e, u_v and a noise obtained by adding GRACE error with a zero mean random white noise between $\pm 0.5\,\mathrm{mm/yr}$. We assume that u is observed by GNSS, and gravitational potential is observed by GRACE. Hence, we can rewrite (7) as:

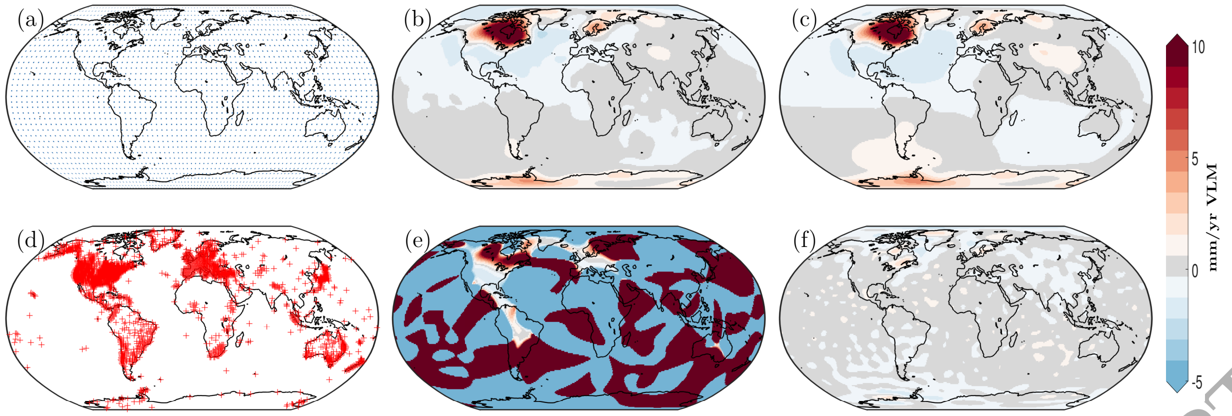

Figure 2. (a) shows the global distribution of synthetic VLM data, where each dot represents a virtual GNSS station. (b) shows the GIA obtained by using (9), (c) shows the background GIA model from Caron et al. (2018) (the truth) that was used for generating the synthetic data, (d) shows the location of GPS stations whose data is available through NGL, (e) shows the GIA obtained by using equation (9) for stations shown in (d), and (f) is the difference between (b) and (c), our closed-loop estimate and the truth (GIA from Caron et al. (2018)). Please note that both (b) and (c) have been smoothed with a Gaussian 500 km filter.

$$
\begin{aligned}
&\Delta\dot{u}(\cdot) - R\sum_{\ell,m}^{L}\left\{\frac{h'_\ell}{1+k'_\ell}\,\tilde{P}_{\ell m}(\cos\theta)\left[\Delta\dot{C}_{\ell m}\cos(m\lambda)+\Delta\dot{S}_{\ell m}\sin(m\lambda)\right]\right\}\\
&= R\sum_{\ell,m}^{L}\left\{\left(1.1677\ell - 0.5233 - \frac{h'_\ell}{1+k'_\ell}\right)\tilde{P}_{\ell m}(\cos\theta)\left[\Delta\dot{C}^{G}_{\ell m}\cos(m\lambda)+\Delta\dot{S}^{G}_{\ell m}\sin(m\lambda)\right]\right\}.
\end{aligned} \tag{9}
$$

For n GNSS stations, the left hand side of (9) represents a $(n \times 1)$ observation vector Y, and the right hand side is $A\,x$, with x being the set of SH coefficients for GIA that can be solved using singular value decomposition (Golub and Reinsch, 1971) or by applying Moore-Penrose inverse for inverting the design matrix. We have used the Moore-Penrose inverse to find a stable solution. Similarly, eqn (8) can be solved to estimate SH coefficients for PDSMC trend instead of GIA.

Imagine a network of GNSS stations 5 degrees apart covering the Earth's surface homogeneously (see Figure 2(a)). In this case, we can solve for SH coefficients up to maximum degree L of 39 (we choose to go up to 35) because the maximum degree L depends on the spatial coverage of the dataset (Colombo, 1981). Such a homogeneous network is the ideal case where we are able to obtain a GIA field which is the same as the truth in the closed-loop setup (see Figure 2(b), (c), and (e)). However, in real world the GNSS network is sparse and there are large regions that are not covered by even a single GNSS station (see Figure 2(d)). This results in a poor estimate of GIA when using the Least-Squares regression (see Figure 2(e)). Since a lot of GPS stations are available in North America and in Europe (the two regions with strongest GIA signal), augmenting GNSS data with synthetic data (obtained from a dedicated GIA model and GRACE data) over regions with poor data availability and small GIA signal can help us overcome the problem with data sparsity. This approach is equivalent to using a prior information from a model and updating it with observations (Sha et al., 2019). It is to be noted that the equi-angular distribution of GPS data leads to latitude weighted regularization; the higher latitudes have relatively higher density of GPS stations and if a majority of them are virtual GPS stations with synthetic VLM then the impact of prior will be larger on the solution. There is an excellent network of GPS stations over American continents, Australia, and the Europe (see Figure 2(d)) (Blewitt et al., 2018). Additionally, GNET and ANET are providing some coverage along the coast of Greenland and Antarctica respectively (Martín-Español et al., 2016; Khan et al., 2016). Hence we have sufficient GPS coverage in high latitude regions where GIA signal is suspected, leading to a larger role of observations and small to negligible impact of the prior on our GIA estimates.

3 ESTIMATING GIA AND PDSMC TRENDS FROM GPS AND GRACE

Several GPS stations are located in tectonics dominated regions and some are affected by other local processes (such as poro-elastic deformations and local geological subsidence or uplift) (Argus et al., 2020). Therefore, GPS time series should be carefully selected so that they represent the physical processes we are interested in, then we can capture GIA or PDSMC with the framework developed in this study.

3.1 GPS data

We use the GPS time series provided by the Nevada Geodetic Laboratory (NGL) in the IGS14 reference frame (Blewitt et al., 2018). The NGL also provides a list of possible offset dates for each GPS station, based on earthquakes occurrence and station maintenance. We complement this list using an offset detection algorithm inspired by MIDAS (Blewitt et al., 2016) in a 2-year sliding window to flag potential offsets when the estimated trend varies abruptly. After correcting for atmospheric loading⋆ and polar motion (King and Watson, 2014), we estimate the annual, semi-annual and linear trend components at each station, for the period January 2005 to December 2015, along with the offsets correction. We only keep stations with at least 3 years of data over this decade because the trend estimated from short time series may not be representative of the long term secular change. Stations with large trends (50 mm/yr or above), large relative uncertainty (trend uncertainty larger than the trend itself) and other outliers are removed, as well as stations located in regions with strong tectonic but weak GIA signal (Japan, Taiwan, Philippines, Indonesia, New Zealand). Stations on oceanic islands are also removed because their signal is expected to be strongly influenced by the nearby ocean or local processes (e.g. volcanic activity). In addition, we manually inspect all the time series and remove the few remaining stations with problems which have not been detected in the previous steps (dubious offsets, remaining outliers, poor signal-to-noise ratio, etc.). Finally, for each station, we use nearby stations (within a radius of 100 km, when available) to look for outliers. If a station has a trend 50% or 5 mm/yr larger or smaller than the median trend of its surrounding stations, we exclude it. This step is equivalent to a smoothing filter and remove the latest outliers in the data set (Schumacher et al., 2018). Hence after the rigorous scrutiny of nearly 10 000 NGL stations, we are left with about 6 000 NGL stations that we use in this study. The list of these stations can be found along with our scripts and dataset at `https://github.com/WhythiskolaveriD/GIAinv.git`.

3.2 GRACE data

The level 2 GRACE time series from IFG, Graz is employed (Mayer-Gürr et al., 2018). The poor quality C_{20} in GRACE is replaced with high quality SLR C_{20} Cheng et al. (2013), and degree one coefficients from Swenson et al. (2007) were included. The time series of SH coefficients between January 2005 and December 2015 are decomposed in terms of an annual, a semi-annual, and a linear trend. The length of time series is limited by poor GPS data availability prior to 2005

⋆ MERRA2 atmospheric model provided by the Loading Service: `http://massloading.net/atm/index.html`

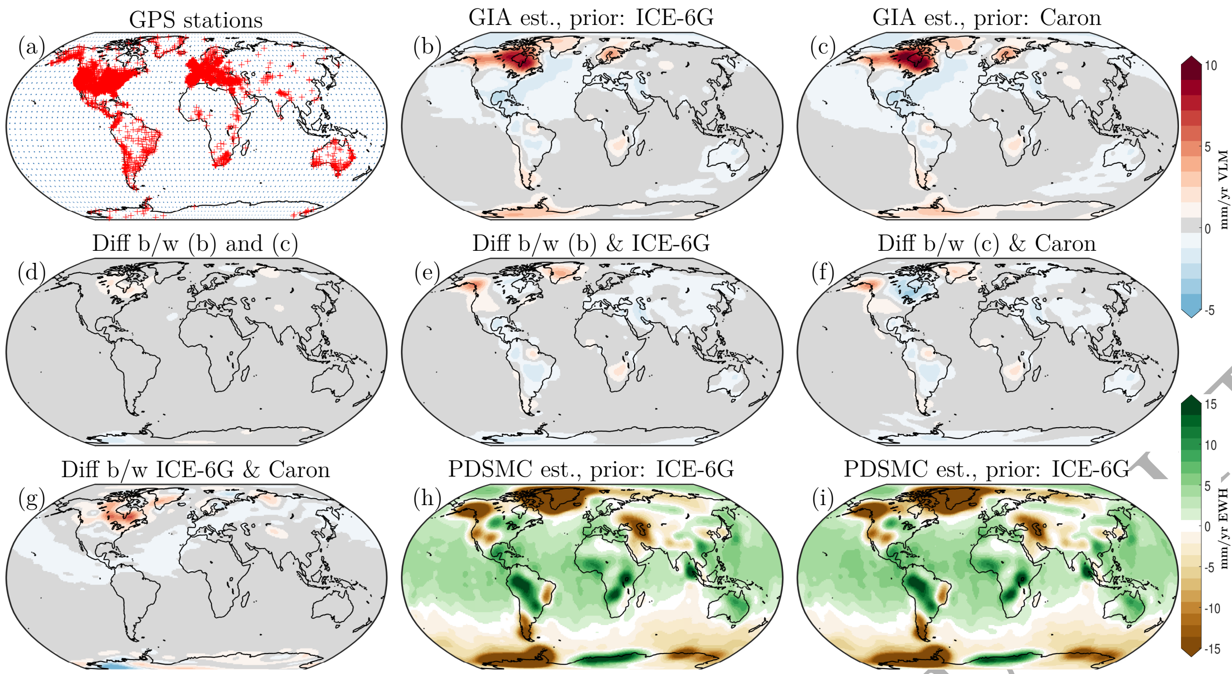

Figure 3. (a) shows the location of NGL GPS stations (red cross) and grid cells where virtual stations with synthetic VLM data (blue dot) were used. (b) shows the GIA VLM obtained by using equation (7) with synthetic data derived from ICE-6G GIA fields and GRACE dataset, (c) is same as (b) but with GIA model from Caron et al. (2018), (d) shows the difference between (b) and (c), (e) shows the update on ICE-6G GIA, which is the difference between (b) and ICE-6G model. (f) is same as (e) but for GIA model from Caron et al. (2018). (g) is the difference between GIA from ICE-6G and Caron et al. (2018). (h) is the PDSMC obtained by using equation (8) with synthetic data derived from ICE-6G GIA fields and GRACE dataset, and (i) is same as (h) but with synthetic data derived using GIA model from Caron et al. (2018). The fields in (b), (c), (h), and (i) are smoothed with a Gaussian 500 km filter for better visualization.

and poor quality of GRACE data after 2015. Since the level 2 GRACE data are noisy, a Gaussian 400 km filter was used (Wahr et al., 1998; Vishwakarma et al., 2016). The trend in SH coefficients are then used in (7) or (8) along with GPS VLM rates, and augmented by synthetic VLM for regions with no reliable observations to obtain the observation vector (left hand side) in (9). The synthetic VLM data are computed by assuming that only GIA and elastic process related VLM are observed and all other processes that may also be captured by a real GPS station are ignored. This benefits the framework in signal separation.

3.3 Results

Figure 3 summarizes the results. In this study we have estimated SH coefficients from degree and order 2 to 35. We ensure conservation of mass by forcing degree 0 to be zero as it should be for GIA estimates. The synthetic VLM rates are computed in the Centre of Figure frame (Blewitt, 2003). Since our synthetic dataset are five degrees apart in regions where we do not have any GPS coverage, we cannot go higher than degree 39, and we choose 35 to ensure the system is solvable. In Figure 3, sub-figure (a) shows the GPS stations used in this study along with locations of synthetic VLM data. (b) and (c) show the GIA estimate obtained when using ICE-6G model and the Caron et al. (2018) GIA model respectively for generating the synthetic VLM data (equivalent to using these models as priors). (d) shows the difference in our GIA estimate when switching between priors, which when compared to the absolute difference in prior (g), is very small and below the uncertainty. To further test the sensitivity of our estimates to a change in prior, four significantly different priors were used. In Figure 4, we show these priors, corresponding GIA estimated from our method, change in prior with respect to the ICE_6G model and respective change in GIA estimates. It can be clearly seen that the GIA estimates do not change much compared to the change in prior. It is to be noted that where the GPS data availability is good, for example in Fennoscandia, the impact of changing the prior is negligible. The impact of prior is more prominent in regions with poor GPS coverage, as can be seen over Canada where the GIA signal is expected to be strong but has a relatively poor GPS coverage. Still the change in estimated GIA is significantly smaller than the change in prior. Therefore, it can be safely concluded that unless a) the GIA models are extremely poor over a certain region and b) it has a poor GPS coverage, the GIA estimates from our method are reliable. In other words, our GIA estimates are heavily data-driven.

The GIA solution obtained from our method is significantly different from the forward models over Alaska, which has an excellent GPS coverage and recently has been attracting a lot of interest (Jin et al., 2017; Hu and Freymueller, 2019). Since this region is tectonically active, the GPS stations suspected to be affected were removed by discarding GPS time-series with jumps and very large trends that cannot be driven by ice-loading and GIA. It is hypothesized that a visco-elastic signal over Alaska is present due to ice load changes during the little ice age (Larsen et al.,

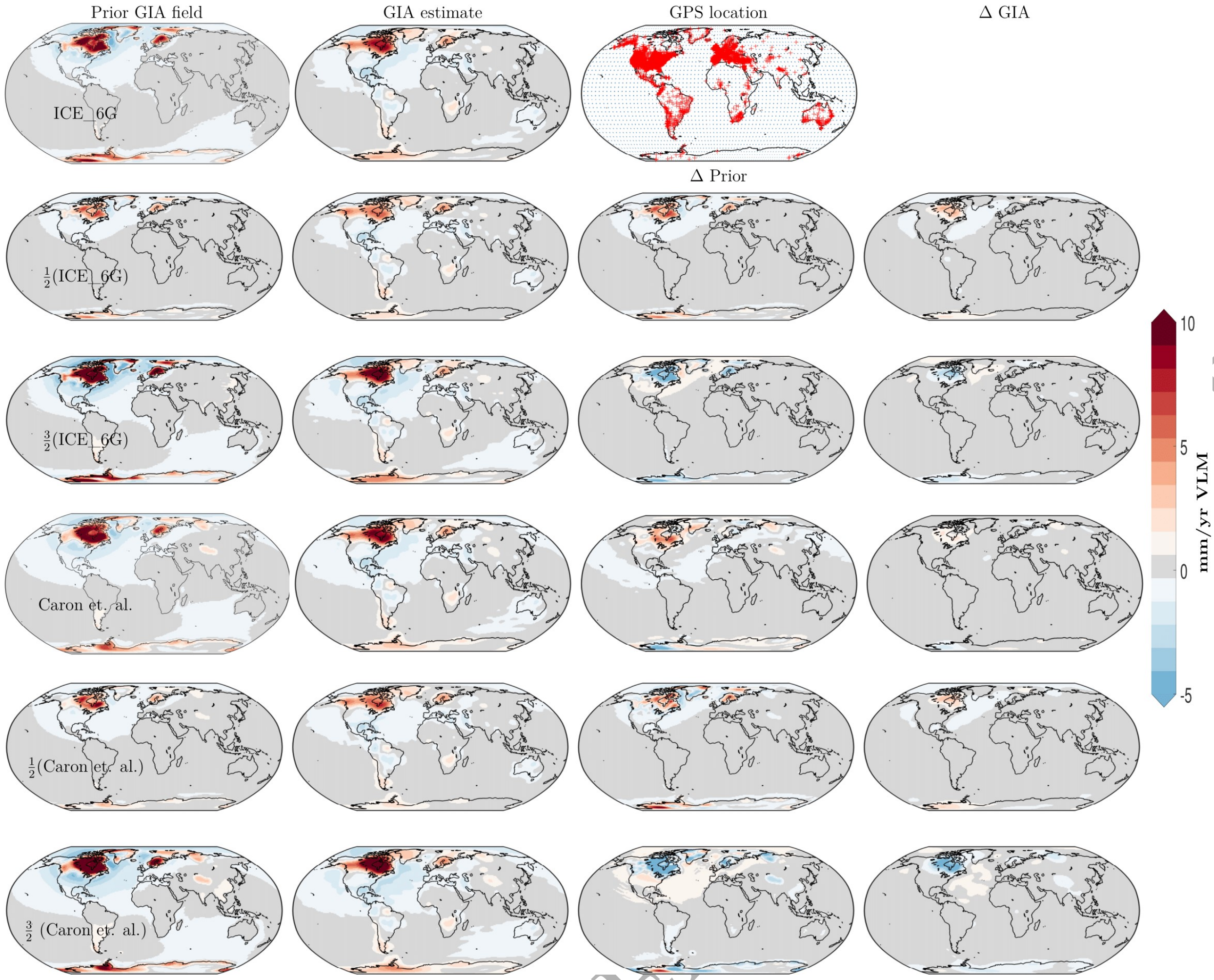

Figure 4. Sensitivity of the GIA solution to change in prior GIA field. The first column shows the prior used. First element in the first row is the ICE_6G model, second is half of the ICE_6G model, third is 150% of the ICE_6G model, the fourth element is the GIA model from Caron et al. (2018), fifth is half of the Caron et al. (2018) GIA model, sixth is 150% of the Caron et al. (2018) GIA model. The second column is the GIA obtained from our method corresponding to the prior in the first column. In the third column, first element shows the location of GPS stations by red cross to provide a perspective on GPS coverage. Second element onward is the change in prior with respect to the ICE_6G model. The fourth column is the change in GIA estimate corresponding to the change in the prior given in the third column.

2005; Sato et al., 2012), which is missed by GIA models. Our estimates show a positive VLM of approximately 5 mm/yr, which is similar to results from Larsen et al. (2005). Our GIA solution is relatively stronger over Greenland and weaker over Antarctica with respect to the two forward model outputs used as prior. Since estimates of GIA over Greenland and Antarctica from different studies vary a lot (Whitehouse, 2018), our result will likely fall in the spread of various GIA estimates.

Some negative signal is obtained over central South-America and a positive signal over southern Africa, which may have been misidentified as GIA either due to presence of local non-viscoelastic signals in GPS data or due to approximations in the relations that were used to convert geo-potential SH coefficients to VLM (in Figure (3) and (2)). In Figure 3, sub-figure (e) and (f) are an update on the respective priors. The ICE-6G estimates over the North America have better agreement with our estimates in comparison with GIA estimates from Caron et al. (2018).

The estimated PDSMC trends (h and i) are consistent with known hydrological trends. The water mass loss over California, High-plain aquifers, Caspian sea, middle east, Northern India, Patagonia, Alaska, Greenland, and Antarctica, are clearly visible (Tapley et al., 2019; Vishwakarma et al., 2020a). The mass gain over Africa, Amazon, Great Lakes, Three Gorges Dam in China, central Antarctica, and Australia are also revealed (Tapley et al., 2019; Vishwakarma et al., 2020a). Hence the mathematical framework is able to separate GIA and PDSMC trends over regions such as Greenland and Antarctica, where the GIA signal is of opposite sign to PDSMC, and it is not affected by large PDSMC signal where GIA is negligible, such as the Caspian Sea, middle-East, and North-west India. Recently GRACE mascon products have become popular as they provide users with ready to use high resolution water mass change estimates (Tapley et al., 2019). These mascon products remove model GIA to obtain PDSMC. Hence the choice of GIA model has an impact on estimated hydrological signal. If we zoom over north America (see Figure 5), we can see that the PDSMC trends from GRACE JPL mascon solution (Watkins et al., 2015), where ICE-6G GIA model was removed, appear to have a hydrological signal over the North-west Canada coinciding with one of the GIA bulge. Such a signal is missing from our PDSMC estimate (Figure 5 (c) and (d)) and our GIA estimate is smaller than ICE-6G in Canada (Figure 3(d)). It is likely that the ICE-6G model overestimates GIA in this region leading to a hydrological signal in GRACE solutions coinciding with the GIA bulge.

The GIA solution from the method demonstrated has a poor spatial resolution for practical purposes, such as using it for removing GIA signal from GRACE data that can be used for hydro-

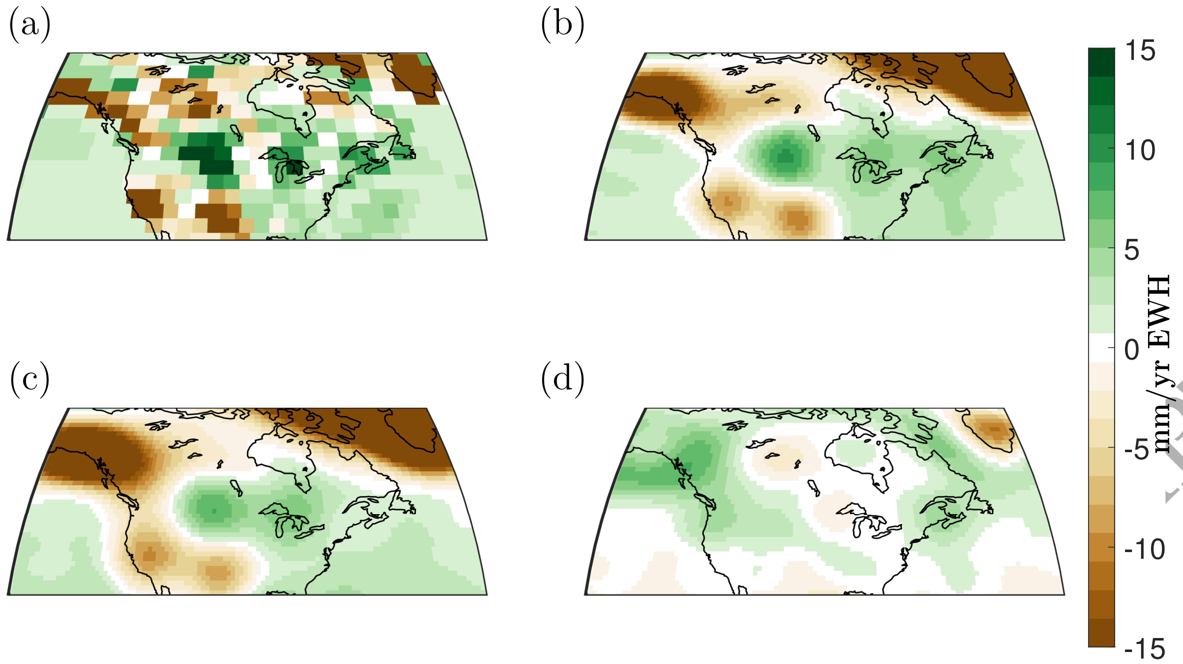

Figure 5. GIA signal in JPL mascons PDSMC (EWH) fields. JPL mascon at 3 degree grid resolution is shown in (a), since they cannot be compared to filtered SH solution, we show a filtered JPL mascon in (b). (c) shows the PDSMC trends from this study and (d) is the difference between (b) and (c).

logical studies, sea level studies, or estimating ice-sheet mass balance at basin scale. Therefore, we propose to improve the spatial resolution artificially by employing the approach by Chen et al. (2015), where a high resolution model is iteratively updated until it's truncated and filtered version matches the GIA estimate from our framework. To ensure that the iterations converge and the output is more meaningful, the regions where we are confident that no GIA process exist have been masked out, conservation of mass is ensured by forcing the degree 0 terms to be zero. The strength of the forward modelling approach is that it starts with a prior and then changes it until its processed version is very close to the observations, hence, the final output can be very different from the prior model wherever the model and observations do not agree. This is the reason, we have a strong GIA signal over Alaska in both the high resolution product as well as the low resolution GIA product from our inversion, while such a signal is not in the prior GIA model. The flow-diagram adapted for our problem is shown in the Fig. 6.

The final high resolution GIA product is shown in the Fig. 7. We have used the ICE-6G model as a prior model here. In Figure 8, we have plotted the degree variance curves for GIA

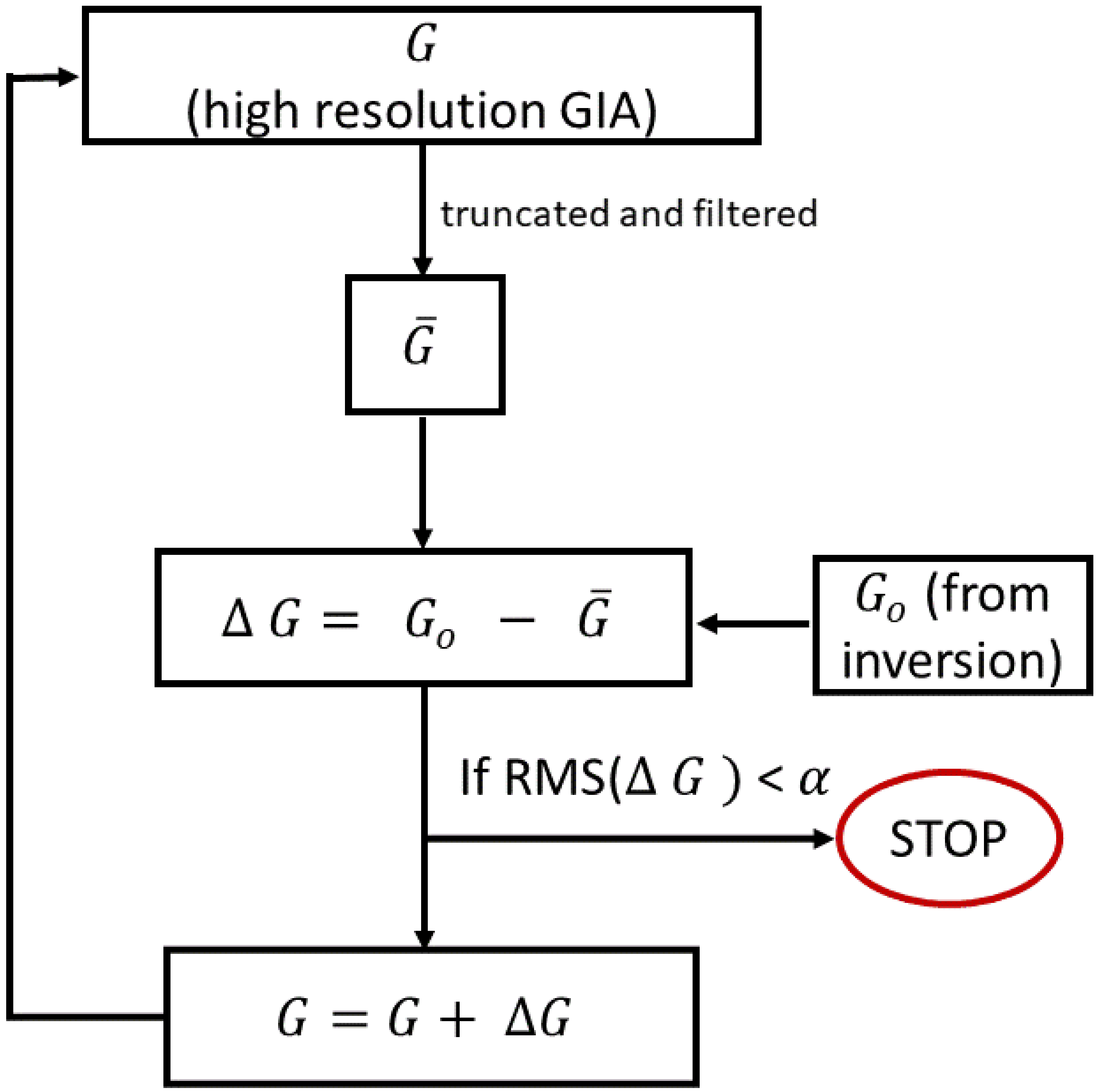

Figure 6. The flowdiagram for the forward modelling approach from Chen et al. (2015) for improving the spatial resolution of the GIA solution. The high resolution GIA model is denoted by G, which when truncated and filtered gives us $\bar{G}$. The difference between $\bar{G}$ and the GIA solution from our inversion (G_o) is computed and added to the GIA model G. This process is repeated until the Root Mean Square of the difference between $\bar{G}$ and G_o is below a threshold α, which was chosen to be 0.1 mm.

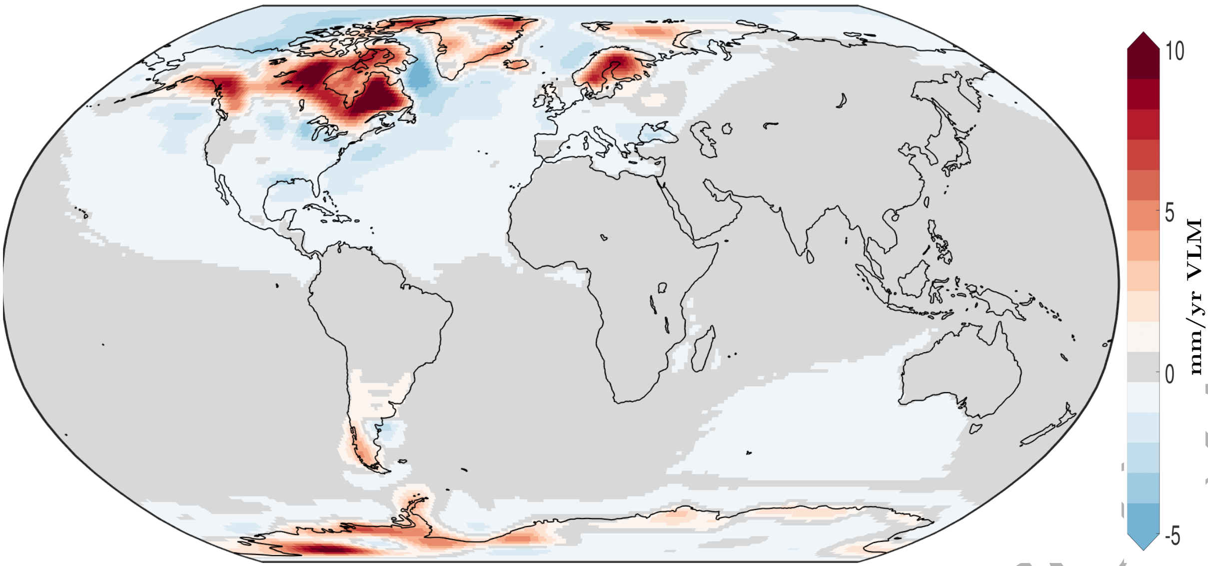

Figure 7. The GIA solution at 1 degree grid sampling.

model from ICE-6G model, our GIA solution, and the high resolution GIA field obtained from the forward modelling approach. The degree variance curves do not deviate significantly, which ensures that the forwarding modelling process does not introduce artificial low degree signals. We share the data, Matlab codes, and outputs from this study via github: `https://github.com/WhythiskolaveriD/GIAinv.git`. Please note that users should be careful in accounting for GIA signal in GRACE at spatial grid scale or commonly known as the level 3 products (for more on this, please see: Vishwakarma et al. (2022)).

3.4 Caveats

The framework presented here relies on approximate relations between SH coefficients and the solid Earth response due to either GIA and PDSMC. These relations were obtained empirically and they work well if the Earth's viscosity profile is spherically symmetric and there are no lateral variations in viscosity of the upper mantle (Wahr et al., 2000; Purcell et al., 2011). Furthermore, these approximate relations, such as that given by Purcell et al. (2011), are only reliable up to a certain degree and order (60 for Purcell et al. (2011)), which means using their relation can not help us capture short wavelength spatial features (represented by higher degree SH coefficients).

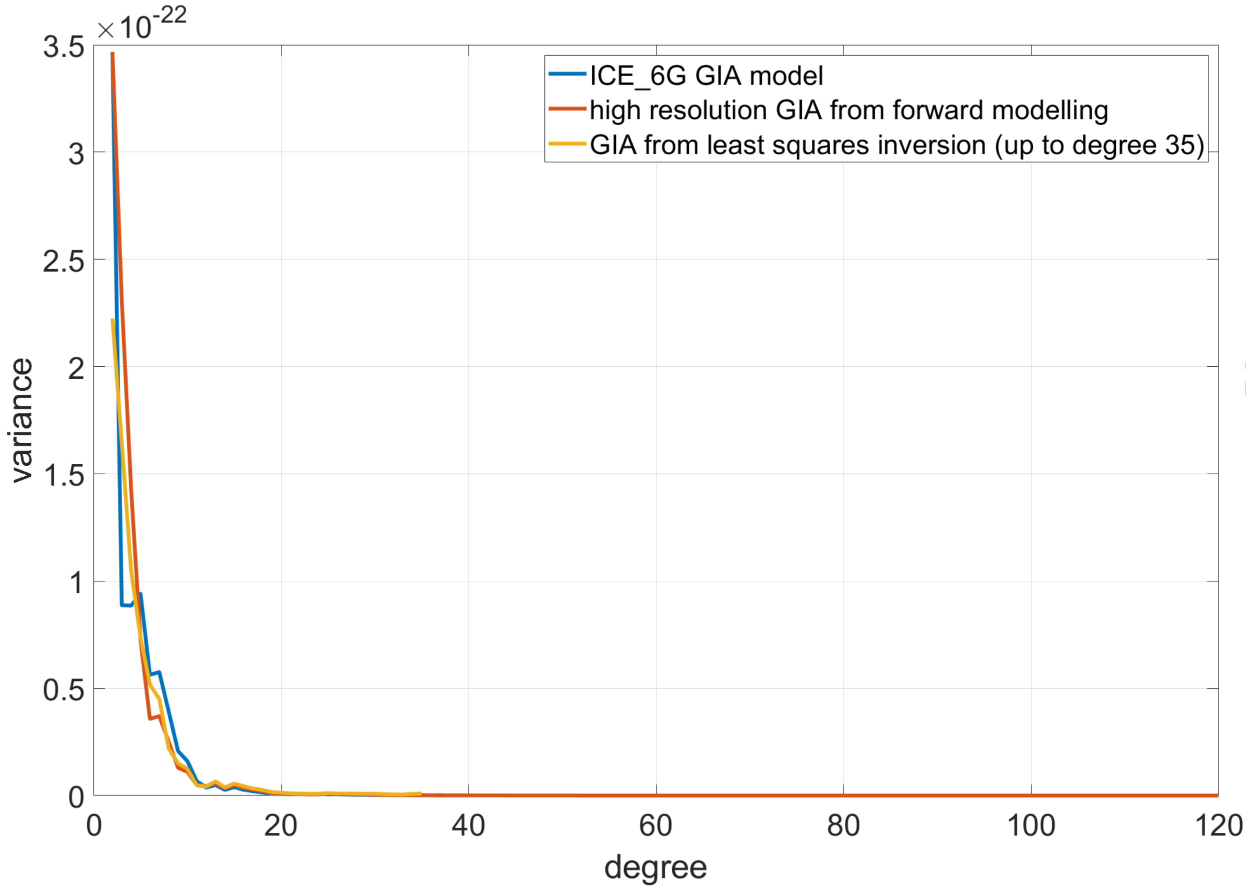

Figure 8. S2: Degree variance curves for ICE_6G GIA model (blue), our GIA solution up to degree 35 (orange), and the high resolution GIA solution obtained with the help of forward modelling (red).

Since we are solving only up to degree and order 35, this limitation does not affect us, but readers that may use our codes on a richer dataset should keep this in mind.

Recent studies have suggested that the viscosity of the upper mantle may vary from one place to another significantly (Barletta et al., 2018), which means that the approximate relations used in this study will not be able to capture such local deviations from a general behaviour. Furthermore, it is assumed that the GPS observes the total of elastic deformations due to PDSMC and the visco-elastic GIA signal only. Any other process that results in VLM is assumed to be negligible. To ensure that this assumption is valid, majority of the stations in tectonically active regions and islands were removed. Nevertheless, some stations in Alaska, South America, and Africa might be affected by our assumption. Therefore, we advise caution on the readers end to interpret our results and use our scripts for processing another dataset. The negative rates in South America and positive rates in southern Africa in our GIA estimate are likely a result of caveats in the method. In our GIA estimates, the strong signal over Alaska matches with recent studies from the GIA community. The GPS coverage and data quality over North America and Europe is excellent, which increases our confidence in our GIA estimates in these regions.

The GIA from our method is only up to degree and order 35 and needs filtering before it can be used for solving geophysical problems. Since, truncation and filtering affect the spatial resolution (Vishwakarma et al., 2018), we must apply a post-processing step to improve the spatial resolution of the GIA gridded dataset. We use the forward modeling approach from Chen et al. (2015), where we ensured that the mass is conserved, the frame of reference is consistent, and suppressing the GIA signal in regions where no signal is suspected, to obtain GIA at 1° grid resolution. The final GIA product can be used for Earth system science.

One of the most difficult part is the uncertainty estimation. Since we are augmenting real GPS data with synthetic data in the spatial domain and then solving the problem to obtain parameters in the SH domain, statistically meaningful propagation of uncertainty is non-trivial. Therefore, we opted for a Monte-Carlo type uncertainty assessment with up to $\pm 50\%$ changes in the amplitude of prior GIA model used to generate the synthetic field. Additionally, we allow the observation vector Y of eqn. (9) to vary within $\pm 20\%$ of its magnitude at a location and solve the model three hundred times to obtain three hundred GIA estimates that are then downscaled using the forward modelling approach. The standard deviation of these outputs is then referred to as the uncertainty in the GIA we obtained, which is shown in the Figure 9. The uncertainty is highest near the main GIA bulge over North America where we expect the largest GIA signal, which can be explained as the allowed variability is a function of percentage of the observation vector and prior GIA magnitude. The uncertainty obtained is comprehensive but a proper error propagation is required that we plan to attempt in another study. The results over Alaska are meaningful because the uncertainty ($\approx$ 0.4 mm/yr) is much smaller than the update on GIA signal (around 5 mm/yr of VLM) with respect to ICE-6G GIA model. Similarly over Greenland the update on GIA is around 2 mm/yr of VLM and the uncertainty is around 0.3 mm/yr. However, over Antarctica, the update is around 2 mm/yr of VLM and the uncertainty is around 1.5 mm/yr, which makes the GIA

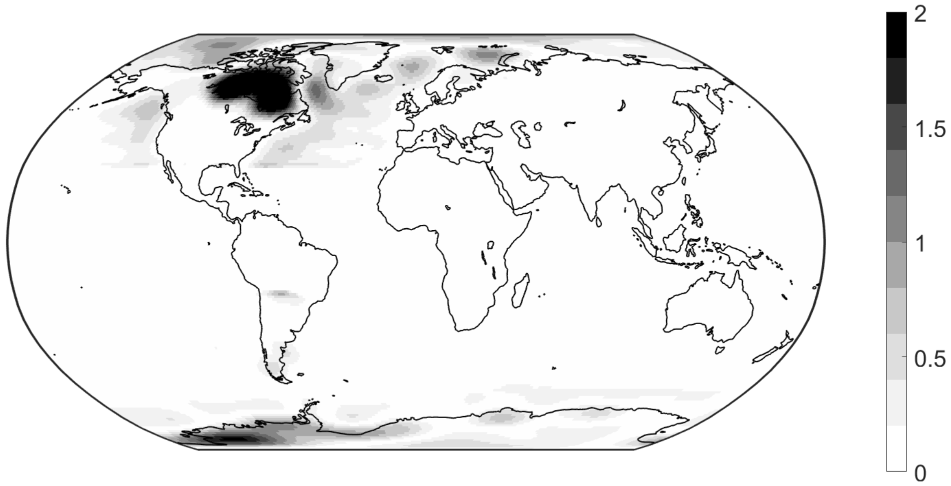

Figure 9. Uncertainty in the estimated high resolution GIA fields. Units are mm/yr VLM.

estimate over Antarctica subject to scrutiny. The uncertainty over Antarctica is still low compared to the absolute magnitudes and once can rely on our estimates as well as on any of the prior GIA model used. A better coverage of GNSS over Antarctica will help us increase accuracy. However, over Alaska and Greenland the results appear reliable. Our results indicate that contemporary Greenland mass change estimates obtained using GRACE and ICE-6G GIA model might be slight overestimated.

4 CONCLUSIONS

Separating the GIA signal from present day surface mass redistribution is a challenging task. In this study, we provide a robust mathematical framework that uses GNSS data and GRACE data to solve this problem. The efficacy of the method is demonstrated in an ideal synthetic closed loop environment. In reality the application of this method is limited by poor spatial coverage of GPS stations. To overcome this limitation, GPS data compiled by the NGL are augmented using virtual GPS stations with synthetic VLM data to estimate the GIA VLM trend and the PDSMC trend between 2005 to 2015. We find that the method is heavily data-driven and not very sensitive to the prior GIA model used for generating synthetic VLM data. The results from our approach agree very well with the general GIA pattern and we observe a significant deviation over Alaska. We also provide data and scripts for users to include more GNSS time-series from additional networks and separate GIA from PDSMC with our data-driven framework.

ACKNOWLEDGMENTS

BDV was supported by the Marie Skłodowska-Curie Individual Fellowship (MSCA-IF) under grant agreement no 841407 (CLOSeR). JLB, YZ, SR were supported by European Research Council (ERC) under the European Union's Horizon 2020 research and innovation programme under grant agreement No 694188, the GlobalMass project (`globalmass.eu`). JLB was additionally supported through a Leverhulme Trust Fellowship (RF-2016-718) and a Royal Society Wolfson Research Merit Award.

All the data used in this study are freely available and have been been downloaded from repositories. The data on which this article is based are available in Blewitt et al. (2018) and Mayer-Gürr et al. (2018). The relevant journal articles, the data set locations, and access dates are provided in the references. The authors are grateful for the open availability of observational data sets. To contribute to the open access of scientific data/method/scripts and to ensure reproducibility we provide Matlab codes and datasets used in this study at: `https://github.com/WhythiskolaveriD/GIAinv.git`.

This work has benefited from many discussions with several experts in the last two years. In particular, we would like to thank Jonathan Rougier from Rougier Consulting Ltd, Erik Ivins from JPL, Martin Horwath and Andreas Groh from TU Dresden, and Ricardo Riva from TU Delft for their insights.

DATA AVAILABILITY

The authors are grateful for the open availability of observational data sets. The source of each data set is cited in the main text. GRACE data and the low degree coefficient time series for GRACE are available at `https://www.tugraz.at/institute/ifg/downloads/gravity-field-models/itsg-grace2018/` and `https://podaac.jpl.nasa.gov/`. GIA data is available at `https://vesl.jpl.nasa.gov/solid-earth/gia/` kindly provided by Caron et al. (2018) and at `https://www.atmosp.physics.utoronto.ca/~peltier/data.php` by Peltier et al. (2015). The MATLAB scripts used to process GRACE spherical harmonic coefficients can be downloaded from `https://www.gis.uni-stuttgart.de/en/research/downloads/`.

References

Argus, D. F., Ratliff, B., DeMets, C., Borsa, A. A., Wiese, D. N., Blewitt, G., Crowley, J. W., Martens, H. R., Kreemer, C., and Landerer, F. W. (2020). Rise of Great Lakes surface water, sinking of the upper Midwest of the United States, and viscous collapse of the forebulge of the former Laurentide ice sheet. *Journal of Geophysical Research: Solid Earth*, 125(9):e2020JB019739.

Barletta, V. R., Bevis, M., Smith, B. E., Wilson, T., Brown, A., Bordoni, A., Willis, M., Khan, S. A., Rovira-Navarro, M., Dalziel, I., et al. (2018). Observed rapid bedrock uplift in Amundsen Sea Embayment promotes ice-sheet stability. *Science*, 360(6395):1335–1339.

Blewitt, G. (2003). Self-consistency in reference frames, geocenter definition, and surface loading of the solid Earth. *Journal of geophysical research: solid earth*, 108(B2).

Blewitt, G., Hammond, W., and Kreemer, C. (2018). Harnessing the GPS data explosion for interdisciplinary science. *Eos*, 99.

Blewitt, G., Kreemer, C., Hammond, W. C., and Gazeaux, J. (2016). MIDAS robust trend estimator for accurate GPS station velocities without step detection. *Journal of Geophysical Research: Solid Earth*, 121(3):2054–2068.

Caron, L. and Ivins, E. R. (2020). A baseline Antarctic GIA correction for space gravimetry. *Earth and Planetary Science Letters*, 531:115957.

Caron, L., Ivins, E. R., Larour, E., Adhikari, S., Nilsson, J., and Blewitt, G. (2018). GIA Model Statistics for GRACE Hydrology, Cryosphere, and Ocean Science. *Geophysical Research Letters*, 45(5):2203–2212.

Chao, B. (2016). Caveats on the equivalent water thickness and surface mascon solutions derived from the GRACE satellite-observed time-variable gravity. *Journal of Geodesy*, 90(9):807–813.

Chen, J., Wilson, C., Li, J., and Zhang, Z. (2015). Reducing leakage error in GRACE-observed long-term ice mass change: a case study in West Antarctica. *Journal of Geodesy*, 89(9):925–940.

Cheng, M., Tapley, B. D., and Ries, J. C. (2013). Deceleration in the Earth's oblateness. *Journal of Geophysical Research: Solid Earth*, 118(2):740–747.

Colombo, O. L. (1981). Numerical methods for harmonic analysis on the sphere. Technical report, Ohio State Univ Columbus Dept of Geodetic Science And Surveying.

Davis, J. L., Elósegui, P., Mitrovica, J. X., and Tamisiea, M. E. (2004). Climate-driven deformation of the solid Earth from GRACE and GPS. *Geophysical Research Letters*, 31(24):L24605.

Farrell, W. and Clark, J. A. (1976). On postglacial sea level. *Geophysical Journal International*, 46(3):647–667.

Farrell, W. E. (1972). Deformation of the Earth by surface loads. *Reviews of Geophysics*, 10(3):761–797.

Gao, C., Lu, Y., Zhang, Z., and Shi, H. (2019). A Joint Inversion Estimate of Antarctic Ice Sheet Mass Balance Using Multi-Geodetic Data Sets. *Remote Sensing*, 11(6).

Geruo, A., Wahr, J., and Zhong, S. (2013). Computations of the viscoelastic response of a 3-D compressible Earth to surface loading: an application to Glacial Isostatic Adjustment in Antarctica and Canada. *Geophysical Journal International*, 192(2):557–572.

Golub, G. H. and Reinsch, C. (1971). Singular value decomposition and least squares solutions. In *Linear algebra*, pages 134–151. Springer.

Gunter, B., Didova, O., Riva, R., Ligtenberg, S., Lenaerts, J., King, M., Van den Broeke, M., Urban, T., et al. (2014). Empirical estimation of present-day Antarctic glacial isostatic adjustment and ice mass change. *The Cryosphere*, 8:743–760.

Hill, E. M., Davis, J. L., Tamisiea, M. E., and Lidberg, M. (2010). Combination of geodetic observations and models for glacial isostatic adjustment fields in Fennoscandia. *Journal of Geophysical Research: Solid Earth*, 115(B7).

Horwath, M., Legrésy, B., Rémy, F., Blarel, F., and Lemoine, J.-M. (2012). Consistent patterns of Antarctic ice sheet interannual variations from ENVISAT radar altimetry and GRACE satellite gravimetry. *Geophysical Journal International*, 189(2):863–876.

Hu, Y. and Freymueller, J. T. (2019). Geodetic observations of time-variable glacial isostatic adjustment in Southeast Alaska and its implications for Earth rheology. *Journal of Geophysical Research: Solid Earth*, 124(9):9870–9889.

Ivins, E. R., James, T. S., Wahr, J., O. Schrama, E. J., Landerer, F. W., and Simon, K. M. (2013). Antarctic contribution to sea level rise observed by GRACE with improved GIA correction. *Journal of Geophysical Research: Solid Earth*, 118(6):3126–3141.

Jin, S., Zhang, T., and Zou, F. (2017). Glacial density and GIA in Alaska estimated from ICESat, GPS and GRACE measurements. *Journal of Geophysical Research: Earth Surface*, 122(1):76–90.

Khan, S. A., Sasgen, I., Bevis, M., van Dam, T., Bamber, J. L., Wahr, J., Willis, M., Kjær, K. H., Wouters, B., Helm, V., et al. (2016). Geodetic measurements reveal similarities between post–Last Glacial Maximum and present-day mass loss from the Greenland ice sheet. *Science advances*, 2(9):e1600931.

King, M. A. and Watson, C. S. (2014). Geodetic vertical velocities affected by recent rapid changes in polar motion. *Geophysical Journal International*, 199(2):1161–1165.

Larsen, C. F., Motyka, R. J., Freymueller, J. T., Echelmeyer, K. A., and Ivins, E. R. (2005). Rapid viscoelastic uplift in southeast Alaska caused by post-Little Ice Age glacial retreat. *Earth and* *planetary Science letters*, 237(3-4):548–560.

Martín-Español, A., Zammit-Mangion, A., Clarke, P. J., Flament, T., Helm, V., King, M. A., Luthcke, S. B., Petrie, E., Rémy, F., Schön, N., et al. (2016). Spatial and temporal Antarctic Ice Sheet mass trends, glacio-isostatic adjustment, and surface processes from a joint inversion of satellite altimeter, gravity, and GPS data. *Journal of Geophysical Research: Earth Surface*, 121(2):182–200.

Mayer-Gürr, T., Behzadpour, S., Ellmer, M., Kvas, A., Klinger, B., and Zehentner, N. (2018). ITSG-Grace2018 - monthly, daily and static gravity field solutions from GRACE. Website, GFZ Data Services. Online available at `https://www.tugraz.at/institute/ifg/downloads/gravity-field-models/itsg-grace2018/`.

Peltier, W. (2004). Global glacial isostasy and the surface of the ice-age Earth: the ICE-5G (VM2) model and GRACE. *Annu. Rev. Earth Planet. Sci.*, 32:111–149.

Peltier, W. (2009). Closure of the budget of global sea level rise over the GRACE era: the importance and magnitudes of the required corrections for global glacial isostatic adjustment. *Quaternary Science Reviews*, 28(17):1658 – 1674. Quaternary Ice Sheet-Ocean Interactions and Landscape Responses.

Peltier, W. R., Argus, D. F., and Drummond, R. (2015). Space geodesy constrains ice age terminal deglaciation: The global ICE-6GC (VM5a) model. *Journal of Geophysical Research: Solid Earth*, 120(1):450–487. 2014JB011176.

Purcell, A., Dehecq, A., Tregoning, P., Potter, E.-K., McClusky, S., and Lambeck, K. (2011). Relationship between glacial isostatic adjustment and gravity perturbations observed by GRACE. *Geophysical Research Letters*, 38(18).

Razeghi, M., Han, S.-C., McClusky, S., and Sauber, J. (2019). A joint analysis of GPS displacement and GRACE geopotential data for simultaneous estimation of geocenter motion and gravitational field. *Journal of Geophysical Research: Solid Earth*, 124(11):12241–12263.

Rietbroek, R., Brunnabend, S.-E., Kusche, J., Schröter, J., and Dahle, C. (2016). Revisiting the contemporary sea-level budget on global and regional scales. *Proceedings of the National Academy of Sciences*.

Riva, R. E. M., Gunter, B. C., Urban, T. J., Vermeersen, B. L., Lindenbergh, R. C., Helsen, M. M., Bamber, J. L., van de Wal, R. S., van den Broeke, M. R., and Schutz, B. E. (2009). Glacial isostatic adjustment over Antarctica from combined ICESat and GRACE satellite data. *Earth and Planetary Science Letters*, 288(3-4):516–523.

Sasgen, I., Martín-Español, A., Horvath, A., Klemann, V., Petrie, E. J., Wouters, B., Horwath, M., Pail, R., Bamber, J. L., Clarke, P. J., et al. (2017). Joint inversion estimate of regional glacial isostatic adjustment in Antarctica considering a lateral varying Earth structure (ESA STSE Project REGINA). *Geophysical Journal International*, 211(3):1534–1553.

Sato, T., Miura, S., Sun, W., Sugano, T., Freymueller, J. T., Larsen, C. F., Ohta, Y., Fujimoto, H., Inazu, D., and Motyka, R. J. (2012). Gravity and uplift rates observed in southeast Alaska and their comparison with GIA model predictions. *Journal of Geophysical Research: Solid Earth*, 117(B1).

Schumacher, M., King, M., Rougier, J., Sha, Z., Khan, S. A., and Bamber, J. (2018). A new global GPS data set for testing and improving modelled GIA uplift rates. *Geophysical Journal International*, 214(3):2164–2176.

Sha, Z., Rougier, J. C., Schumacher, M., and Bamber, J. L. (2019). Bayesian model–data synthesis with an application to global glacio-isostatic adjustment. *Environmetrics*, 30(1):e2530.

Shepherd, A., Ivins, E., Rignot, E., Smith, B., Van Den Broeke, M., Velicogna, I., Whitehouse, P., Briggs, K., Joughin, I., Krinner, G., et al. (2018). Mass balance of the Antarctic Ice Sheet from 1992 to 2017. *Nature*, 558:219–222.

Simon, K. M., Riva, R. E. M., Kleinherenbrink, M., and Tangdamrongsub, N. (2017). A data-driven model for constraint of present-day glacial isostatic adjustment in North America. *Earth and Planetary Science Letters*, 474:322–333.

Sun, Y. and Riva, R. E. M. (2020). A global semi-empirical glacial isostatic adjustment (GIA) model based on Gravity Recovery and Climate Experiment (GRACE) data. *Earth System Dynamics*, 11(1):129–137.

Swenson, S., Chamber, D., and Wahr, J. (2007). Estimating geocenter variations from a combination of GRACE and ocean model output. *Journal of Geophysical Research*, 113:B08410.

Tapley, B. D., Watkins, M. M., Flechtner, F., Reigber, C., Bettadpur, S., Rodell, M., Sasgen, I., Famiglietti, J. S., Landerer, F. W., Chambers, D. P., Reager, J. T., Gardner, A. S., Save, H., Ivins, E. R., Swenson, S. C., Boening, C., Dahle, C., Wiese, D. N., Dobslaw, H., Tamisiea, M. E., and Velicogna, I. (2019). Contributions of GRACE to understanding climate change. *Nat. Clim. Change*, 9:358–369.

Tregoning, P., Ramillien, G., McQueen, H., and Zwartz, D. (2009). Glacial isostatic adjustment and nonstationary signals observed by GRACE. *Journal of Geophysical Research: Solid Earth*, 114(B6).

van Dam, T., Wahr, J., and Lavallée, D. (2007). A comparison of annual vertical crustal displacements from GPS and Gravity Recovery and Climate Experiment (GRACE) over Europe. *Journal of Geophysical Research: Solid Earth*, 112(B3):B03404.

Velicogna, I. and Wahr, J. (2002). A method for separating Antarctic postglacial rebound and ice mass balance using future ICESat Geoscience Laser Altimeter System, Gravity Recovery and Climate Experiment, and GPS satellite data. *Journal of Geophysical Research: Solid Earth*, 107(B10):ETG 20–1–ETG 20–11.

Vishwakarma, B. D., Bates, P., Sneeuw, N., Westaway, R. M., and Bamber, J. L. (2020a). Reassessing global water storage trends from GRACE time series. *Environmental Research Letters*.

Vishwakarma, B. D., Devaraju, B., and Sneeuw, N. (2016). Minimizing the effects of filtering on catchment scale GRACE solutions. *Water Resources Research*, 52(8):5868–5890.

Vishwakarma, B. D., Devaraju, B., and Sneeuw, N. (2018). What is the spatial resolution of GRACE satellite products for hydrology? *Remote Sensing*, 10(852).

Vishwakarma, B. D., Horwath, M., Groh, A., and Bamber, J. L. (2022). Accounting for GIA signal in GRACE products. *Geophysical Journal International*, 228(3):2056–2060.

Vishwakarma, B. D., Royston, S., Riva, R. E. M., Westaway, R. M., and Bamber, J. L. (2020b). Sea level budgets should account for ocean bottom deformation. *Geophysical Research Letters*, 47(3):e2019GL086492.

Wahr, J., Molenaar, M., and Bryan, F. (1998). Time variability of the Earth's gravity field: Hydrological and oceanic effects and their possible detection using GRACE. *Journal of Geophysical Research: Solid Earth*, 103(B12):30205–30229.

Wahr, J., Wingham, D., and Bentley, C. (2000). A method of combining ICESat and GRACE satellite data to constrain Antarctic mass balance. *Journal of Geophysical Research: Solid Earth*, 105(B7):16279–16294.

Wang, H., Jia, L., Steffen, H., Wu, P., Jiang, L., Hsu, H., Xiang, L., Wang, Z., and Hu, B. (2013). Increased water storage in North America and Scandinavia from GRACE gravity data. *Nature Geoscience*, 6(1):38–42.

Watkins, M. M., Wiese, D. N., Yuan, D.-N., Boening, C., and Landerer, F. W. (2015). Improved methods for observing Earth's time variable mass distribution with GRACE using spherical cap mascons. *Journal of Geophysical Research: Solid Earth*, 120(4):2648–2671.

WCRP, G. (2018). Global sea-level budget 1993-–present. *Earth Syst. Sci. Data*, 10:1551–1590.

Whitehouse, P. L. (2018). Glacial isostatic adjustment modelling: historical perspectives, recent advances, and future directions. *Earth surface dynamics*, 6(2):401–429.

Willen, M. O., Horwath, M., Schröder, L., Groh, A., Ligtenberg, S. R., Kuipers Munneke, P., and Van Den Broeke, M. R. (2020). Sensitivity of inverse glacial isostatic adjustment estimates over Antarctica. *Cryosphere*, 14(1):349–366.

Wu, X., Heflin, M. B., Schotman, H., Vermeersen, B. L., Dong, D., Gross, R. S., Ivins, E. R., Moore, A. W., and Owen, S. E. (2010). Simultaneous estimation of global present-day water transport and glacial isostatic adjustment. *Nature Geoscience*, 3(9):642–646.

Zou, F. and Jin, S. (2016). Estimations of glacier melting in Greenland from combined satellite gravimetry and ICESat. In *2016 IEEE International Geoscience and Remote Sensing Symposium (IGARSS)*, pages 6185–6188. IEEE.